Unique aqueous Li-ion/sulfur chemistry with high energy density and reversibility

Chongyin Yang[a], Liumin Suo[a], Oleg Borodin[b], Fei Wang[a], Wei Sun[a], Tao Gao[a], Xiulin Fan[a], Singyuk Hou[a], Zhaohui Ma[a], Khalil Amine[c], Kang Xu[b,1], and Chunsheng Wang[a,1]

[a]Department of Chemical and Biomolecular Engineering, University of Maryland, College Park, MD 20740; [b]Electrochemistry Branch, Sensor and Electron Devices Directorate, Power and Energy Division, US Army Research Laboratory, Adelphi, MD 20783; and [c]Chemical Sciences and Engineering Division, Argonne National Laboratory, Argonne, IL 60439

Edited by Thomas E. Mallouk, The Pennsylvania State University, University Park, PA, and approved May 9, 2017 (received for review March 8, 2017)

Leveraging the most recent success in expanding the electrochemical stability window of aqueous electrolytes, in this work we create a unique Li-ion/sulfur chemistry of both high energy density and safety. We show that in the superconcentrated aqueous electrolyte, lithiation of sulfur experiences phase change from a high-order polysulfide to low-order polysulfides through solid–liquid two-phase reaction pathway, where the liquid polysulfide phase in the sulfide electrode is thermodynamically phase-separated from the superconcentrated aqueous electrolyte. The sulfur with solid–liquid two-phase exhibits a reversible capacity of 1,327 mAh/(g of S), along with fast reaction kinetics and negligible polysulfide dissolution. By coupling a sulfur anode with different Li-ion cathode materials, the aqueous Li-ion/sulfur full cell delivers record-high energy densities up to 200 Wh/(kg of total electrode mass) for >1,000 cycles at ∼100% coulombic efficiency. These performances already approach that of commercial lithium-ion batteries (LIBs) using a nonaqueous electrolyte, along with intrinsic safety not possessed by the latter. The excellent performance of this aqueous battery chemistry significantly promotes the practical possibility of aqueous LIBs in large-format applications.

water-in-salt | rechargeable aqueous battery | aqueous sulfur battery | gel polymer electrolyte | phase separation

In the past two decades, rechargeable lithium-ion batteries (LIBs) have revolutionized consumer electronics with their high energy density and excellent cycling stability, and are the state-of-the-art candidates for applications ranging from kilowatt hours for electric vehicles up to megawatt hours for grids (1, 2). The latter applications in large-format present much more stringent requirements for safety, cost, and environmental friendliness, besides energy density and cycle life. The shortcomings of LIB are mostly due to the flammable and toxic nonaqueous electrolytes and moderate energy densities (<400 $Wh{\cdot}kg^{-1}$) provided by the electrochemical couples currently used (3). Among the various "beyond Li-ion" high-energy chemistries (>500 $Wh{\cdot}kg^{-1}$) explored currently, the nonaqueous lithium/sulfur (Li/S) battery based on sulfur as a cathode (theoretical capacity of 1,675 $mAh{\cdot}g^{-1}$) and metallic lithium as an anode seems to be the most practical, as evidenced by the mushrooming literature and significant advances in this system in the past 5 y (4–7). However, commercialization of this system still faces challenges because of severe safety concerns associated with the dendrite growth of metallic Li anode in highly inflammable ether-based electrolytes (8), and the high self-discharge associated with parasitic shuttling of the intermediate polysulfide species. Moreover, the moisture-sensitive nature of the nonaqueous electrolyte would contribute significantly to the cost of the Li/S battery pack due to the stringent moisture-exclusion infrastructure required during the manufacturing, processing, and packaging of the cells. The indispensable accessories for safety and thermal management would further drive up the cost.

Replacement of the nonaqueous electrolyte by its aqueous counterpart is always tantalizing, because it would essentially eliminate safety, toxicity, and at least part of the cost concerns (9–11). In particular, wide electrochemical stability windows (>3.0 V) comparable to those of nonaqueous electrolytes have been recently demonstrated by water-in-salt (WiS) and water-in-bisalt (WiBS) electrolytes. With water molecules still far outnumbering that of Li salts, this class of completely nonflammable WiS and WiBS electrolytes realized a dramatic improvement in safety, while placing many Li-ion and even beyond Li-ion chemistries within the reach of aqueous electrolytes (12, 13). Historically, it has been very challenging to use elemental sulfur as the cathode material in aqueous electrolytes, primarily because of the high solubility of short-chain lithium polysulfide (Li_2S_x, $x < 6$) and Li_2S in aqueous media, and the strong parasitic shuttling reaction occurring thereafter (14). A compromise approach used aqueous solution of lithium polysulfide as the liquid active cathode (catholyte), but only 61% of the theoretical capacity was accessed in the Li_2S_4/Li_2S redox couple (15–17). The hydrogen evolution in this aqueous system and the side reaction between the Li_2S_4/Li_2S and H_2O have to be suppressed to achieve high coulombic efficiency. A Li metal anode can be used, but only after a dense Li-ion-conducting ceramic layer is engineered on the Li surface to prevent Li dendrite formation and prevent the reaction of Li anode from aqueous catholyte (17).

However, the reported electrochemical stability windows of the superconcentrated aqueous electrolytes (WiS, WiBS) were >3.0 V, with cathodic and anodic limits located in the vicinity of ∼1.9 V and ∼4.9 V vs. Li, respectively. This window would comfortably envelop the lithiation/delithiation reactions of high-capacity

Significance

Sulfur as an anode coupled with a lithium-ion intercalation cathode in the superconcentrated aqueous electrolyte creates a unique Li-ion/sulfur chemistry, realizing the highest energy density ever achieved in aqueous batteries, along with high safety and excellent cycle-life. Mechanism investigation finds that the reversible sulfur lithiation/delithiation in such an aqueous electrolyte proceeds with fast kinetics that significantly differ from that in nonaqueous systems, whereas polysulfides' insolubility in such an aqueous electrolyte essentially eliminates the parasitic shuttling. The excellent performances of Li-ion/sulfur cells not only find an application of "water-in-salt" electrolyte for beyond Li-ion chemistries, more importantly, an alternative pathway is provided to solve the "polysulfide shuttling" that has been plaguing the sulfur chemistries in nonaqueous electrolytes.

Author contributions: C.Y., L.S., O.B., F.W., K.A., K.X., and C.W. designed research; C.Y., L.S., O.B., F.W., W.S., T.G., X.F., S.H., and Z.M. performed research; C.Y., O.B., F.W., W.S., T.G., X.F., S.H., Z.M., K.A., K.X., and C.W. analyzed data; and C.Y., L.S., O.B., F.W., S.H., K.A., K.X., and C.W. wrote the paper.

The authors declare no conflict of interest.

This article is a PNAS Direct Submission.

[1]To whom correspondence may be addressed. Email: cswang@umd.edu or conrad.k.xu.civ@mail.mil.

This article contains supporting information online at www.pnas.org/lookup/suppl/doi:10.1073/pnas.1703937114/-/DCSupplemental.

sulfur materials at the anode side and transition metal oxide materials at the cathode side. The electrochemical coupling of a sulfur anode and an intercalation cathode would thus create a new cell chemistry without Li metal, which is based on Li^+ intercalation/deintercalation at the cathode, and conversion reaction of sulfur species at anode. This Li-ion/sulfur chemistry (Li^+/S) can deliver theoretic energy densities up to 260 Wh·kg^{-1}, and combines the high capacities of a cheap sulfur anode and mature LIB cathode, as well as the intrinsic safety of an aqueous electrolyte. Additional benefits include substantial cost reduction at the battery module or pack level, via elimination of moisture-free infrastructures for processing and fabrication, and the possible simplification of the safety management.

In this work, we demonstrate this highly reversible aqueous Li^+/S chemistry using a simple sulfur/carbon composite as the anode and LiMO ($LiMn_2O_4$ and $LiCoO_2$) as the cathodes. Through in situ and ex situ spectroscopic means during electrochemical reactions, the unique lithiation/delithiation mechanism of sulfur in WiBS electrolyte was revealed to proceed reversibly in a solid–liquid phase. A total of 80% (1,327 mAh·g^{-1}) of sulfur theoretical capacity (1,675 mAh·g^{-1}) was accessed with excellent reversibility, as evidenced by capacity retention of 86% for 1,000 cycles. This outstanding performance is attributed to the phase separation of S/polysulfide solid–liquid phase from high-concentration aqueous electrolytes, where the liquid WiBS electrolyte functions in a similar manner as solid electrolyte in isolating the polysulfide species generated at anode from LiMO cathodes, thus eliminating the parasitic shuttlings that have been plaguing the nonaqueous Li/sulfur chemistry. When the sulfur anode was paired with typical LIB cathode materials like $LiMn_2O_4$ or high-voltage $LiCoO_2$, energy densities of 135~200 Wh·kg^{-1} were delivered at full cell level. These findings suggest that safety, cost, environmental considerations, and energy density requirements could be simultaneously achieved by the aqueous Li^+/S battery for large-scale applications, such as smart-grid storage or automotive power systems.

Results

Electrochemical Behaviors of Sulfur in WiBS Aqueous Electrolyte. The electrochemical behaviors of a sulfur–Ketjen black (S-KB) carbon composite electrode in WiBS electrolyte and in typical organic electrolyte were investigated with cyclic voltammetry. WiBS electrolyte was obtained by dissolving two Li salts, lithium bis(trifluoromethane sulfonyl)imide (LiTFSI) and lithium trifluoromethane sulfonate (LiOTf) at 21 and 7 mol·kg^{-1}, respectively, in water at 25 °C. Using two lithium salts allows us to circumvent the solubility limits of each single lithium salt in water, hence reaching the highest salt concentration possible (13, 18). The extremely high concentration therein provides an expanded stability window thanks to the formation of a dense and protective solid electrolyte interphase (SEI) and the reduced water activity (13); it is also a key to manage stable phase-separation of liquid reaction intermediate and liquid electrolyte, which will be fully discussed below. Reversible lithiation/delithiation reaction of sulfur in this 28-mol·kg^{-1} electrolyte was observed at 2.46 and 2.65 V, respectively (Fig. 1*A*). Although the potential for hydrogen evolution at pH ~7.0 is known to be ~2.63 V vs. Li, the SEI suppresses the reduction of water molecules down to the potential of ~1.9 V, hence making the reversible lithiation/delithiation reaction possible. Upon closer comparison with the well-known redox processes of sulfur in nonaqueous media at 2.1~2.4 V (Fig. 1*A*, black dashed line) (19), an apparent positive shift of ~0.3 V occurred in the aqueous solution, which has been observed previously and attributed to the high Li salt concentration in WiBS electrolyte (12). More noticeable is the drastic change from the characteristic two-stage lithiation process in nonaqueous media to a seemingly single-stage redox process in aqueous media, as well as the much reduced potential hysteresis in the latter. Such changes are more visually obvious in the corresponding voltage profiles obtained in galvanostatic mode (Fig. 1*B*), where a single, well-defined plateau at ~2.5 V represents the discharge/charge of S-KB in the WiBS electrolyte, significantly differing from the two plateaus found at ~2.3 and 2.1 V in nonaqueous electrolyte (20). Apparently, the electrochemical reaction of sulfur in this superconcentrated aqueous electrolyte proceeds via a new reaction mechanism that is hitherto unknown. What we see in Fig. 1 should be a previously unobserved aqueous sulfur chemistry.

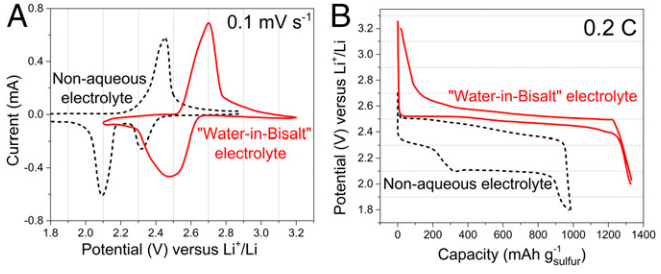

Fig. 1. Electrochemical performance of sulfur in aqueous electrolyte. (*A*) Cyclic voltammograms of S-KB composite at 0.1 mV·s^{-1} in aqueous electrolyte (red solid line) and nonaqueous electrolyte (black dashed line). (*B*) Typical voltage profiles of S-KB composite at constant current (0.2C) in aqueous electrolyte (red solid line) and nonaqueous electrolyte (black dashed line).

The typical two-plateau discharge curve obtained in nonaqueous media has been attributed to the solid-to-liquid (sulfur to dissolved high-order polysulfide) reaction, and liquid-to-solid (high-order polysulfides to low-order sulphide solid) reaction (21–23). The single-stage discharge plateau in WiBS electrolyte, however, suggested that the redox processes of sulfur undergo a single solid–liquid reaction, which proceeds with ultrafast kinetics; this is also consistent with the finding of Li_2S product formed during early charging, as discussed hereafter. As a result, a reversible capacity of 1,338 mAh·g^{-1} was achieved based on the sulfur mass at a current density of 335 mA·g^{-1} (0.2C), which is 80% of the theoretical capacity and comparable with the best results achieved in nonaqueous electrolyte (4).

Reaction Mechanism of Sulfur Anode in WiBS Electrolyte. To fully understand this sulfur chemistry in WiBS electrolyte, we used in situ Raman spectroscopy to monitor the transformation of polysulfide species in the S-KB anode at different states of charge (SOC) during the third charge of an S-KB/$LiMn_2O_4$ full cell (Fig. 2*A*). The fully discharged (delithiated) S-KB anode (SOC = 0%, corresponding to the fully charged state of sulfur when used as cathode in nonaqueous electrolyte) showed conspicuous peaks (indicated by yellow region in Fig. 2*A*) corresponding to elemental sulfur (α-S_8) at 81, 151, 217, and 470 cm^{-1} (24). Based on the normalized intensity ratio, the estimated amount of α-S_8 exponentially declines to nearly zero before the SOC reaches 25%, suggesting a surprisingly rapid and full consumption of S_8 by lithiation (Fig. 2*C*). A sharp peak at 339 cm^{-1}, which was assigned to the long-chain polysulfide species S_6^{2-} (25, 26), appeared at SOC = 25% but disappeared after SOC = 75%. Meanwhile, a small peak at 234 cm^{-1}, which was attributed to the bending mode of S_4^{2-}, gradually grew after SOC = 25% during charge (27). At the final stage of charge (SOC = 100%), a Li_2S peak located at 371 cm^{-1} appeared. These results clearly show the very rapid procession from elemental sulfur to long-chain polysulfides and then to the fully lithiated form Li_2S (i.e., S_8 → long chain Li_2S_x → short chain Li_2S_x → Li_2S). The fast kinetic drastically differs from the reduction of sulfur in nonaqueous media. In the aqueous media, an obvious lift-up occurs in the range of 65–300 cm^{-1} (Fig. 2*A*) with a peak at 80 cm^{-1} for SOC ≥ 50%. To investigate these peaks further, the Raman spectra of

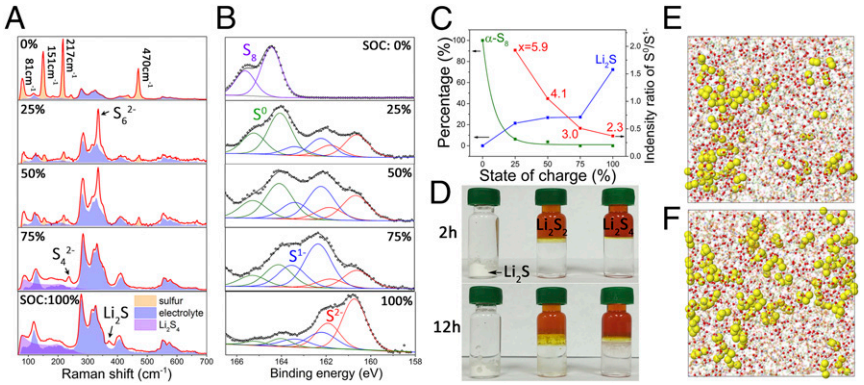

Fig. 2. In situ and ex situ studies of redox intermediate for sulfur anode. (*A*) In situ Raman spectra of the S-KB anode in full cell after being charged to specific SOC. Red lines are experimental data, and colored areas correspond to deconvoluted individual components. (*B*) XPS S 2*p* spectra of S-KB anode in full cell after being charged to specific states. Black dotted lines are experimental data, black lines are overall fitted data, and colored solid lines are fitted individual chemical states: $2p_{3/2\text{-purple}}(S_8)$ 164.4 eV; $2p_{3/2\text{-green}}(S^0)$ 164.0 eV; $2p_{3/2\text{-blue}}(S^{1-})$ 162.2 eV; and $2p_{3/2\text{--red}}(S^{2-})$ 160.7 eV. (*C*) The estimated content ratios of element S_8 (green), Li_2S (blue), and LiPS at specific SOCs. (*D*) Visual observation of the insolubilities for Li_2S and short-chain LiPS (Li_2S_2 and Li_2S_4) in WiBS electrolyte. A Li_2S white powder remains insoluble in clear aqueous electrolyte for 12 h. Jacinth solution on the top of bottle is Li_2S_2 or Li_2S_4 dissolved in water phase, which is separated from the clear aqueous electrolyte (salt phase) on the bottom. (*E* and *F*) Projections of MD simulation boxes highlighting Li_2S_4 (*F*) and Li_2S_2 (*E*) polysulfide anions (yellow) and water (O, red; H, white) separating in WiBS electrolyte at 333 K, respectively.

element sulfur powder, pure Li_2S powder, Li_2S_4 in aqueous solution, and WiBS electrolyte were analyzed (*SI Appendix*, Fig. S1). The peaks in the range of 65–300 cm^{-1} with a peak at 80 cm^{-1} for the S-KB anode were well fitted to the Raman spectra of water-solvated polysulfide mixture (Li_2S_4, purple area). Therefore, the Li_2S_4 manages to extract H_2O from WiBS electrolyte to form a Li_2S_4-anolyte, which is immiscible with the bulk WiBS electrolyte (Fig. 2*D*). Note that the dissolved lithium polysulfide (LiPS) only shows a wide peak at 80 cm^{-1}. Hence, sharp peaks for S_6^{2-} at SOC = 25% and for S_4^{2-} at SOC = 75% can only be attribute to solid phase of LiPS. A more direct observation of solid–liquid mixed polysulfide phase was confirmed by replacing an S-KB anode with sulfur coated on aluminum mesh (denoted as S@Al hereafter) that was horizontally placed on the top surface of WiBS electrolyte. The Raman spectra of the charged S@Al electrode showed individual traces of both liquid and solid polysulfide (*SI Appendix*, Fig. S2). This observation unambiguously reveals that the reaction intermediate (polysulfide) exist in both solid and liquid phase, where the liquefied polysulfides would have been confined by pore structure of carbon matrix and hence phase separated from WiBS in our full cells. Further confirmations of solid–liquid mixed phase of S-KB came from the electrochemistry performances of the washed S-KB at different SOC (*SI Appendix*, Fig. S3). After charging to states of 50%, 75%, and 100%, the S-KB electrodes were disassembled and washed using anhydrous dimethoxyethane (DME) for serval times to remove the liquid polysulfides, and then reassembled to measure the residual low-order solid polysulfides. After removing liquid phase and long-order LiPS intermediate, the remaining low-order solid polysulfides still can provide >70% of initial capacities. In diluted aqueous solutions, the long-chain species Li_2S_x ($x > 4$) are considered insoluble due to their relatively less-polar nature, whereas the short-chain species Li_2S_x ($x \leq 4$) are highly soluble (over 4 M) due to their higher ionic nature (15, 17). However, both species become insoluble in WiBS electrolyte due to the high lithium salt concentrations. Molecular dynamics (MD) simulations of Li_2S_2 and Li_2S_4 in WiBS electrolyte revealed that these polysulfides severely aggregate, resulting in obvious domain formation in WiBS as shown in Fig. 2 *E* and *F*, with shorter polysulfide yielding more pronounced aggregation. Quantum chemistry calculations predicted higher stability of Li_2S_2 vs. Li_2S_4 in aqueous environment as discussed in *SI Appendix*. Preferential stability of shorter polysulfide Li_2S_2 vs. Li_2S_4 together with their stronger aggregation and separation is consistent with the experimentally observed phase separation of polysulfides in WiBS electrolyte. MD simulations also show that the short-chain Li_2S_x ($x \leq 4$) can indeed extract water molecules from the superconcentrated WiBS electrolyte until reaching equilibrium with WiBS, forming a mixed solid and liquefied anolyte, which is not miscible with the bulk WiBS electrolyte. Hence, the lithiation state of the sulfur anode in WiBS electrolyte should maintain solid–liquid mixed phase, in accordance with the previous electrochemical behavior. Thanks to the immiscibility of saturated Li_2S_x ($x < 4$) anolyte with WiBS electrolyte, the parasitic shuttle reactions of the polysulfides that have been plaguing the nonaqueous Li/S chemistry are effectively suppressed.

X-ray photoelectron spectroscopic (XPS) analysis was also conducted on the S-KB anodes retrieved from the full cells at different SOCs of the third charge (Fig. 2*B*). For clarity, only the $2p_{3/2}$ component of the S $2p_{3/2}/2p_{1/2}$ doublet was analyzed. Because the peaks at the binding energy over 166 eV are dominated by the contributions from LiTFSI and LiOTf salt anion residuals, as demonstrated in *SI Appendix*, Fig. S4, only the spectra in the range of 158–166 eV were selected to fit the S2*p* of S_8, S^0, S^{1-}, and S^{2-} (Fig. 2*B*) (28, 29). At SOC = 0%, only S_8 (164.4 eV) was observed, whereas polysulfide species S_x^{2-} ($8 \geq x \geq 2$) appeared during lithiation, which were fitted with S^0 at 164.0 eV and S^{-1} at 162.2 eV, respectively. In the chain structure of S_x^{2-} species, the two terminal sulfur atoms at both ends bear a formal charge of −1, with several bridging sulfur atoms in the middle bearing a formal charge of zero. The average oxidation states were thus determined by the ratio of terminal/bridging sulfur peaks, leading to an average lithium polysulfide formula approximately equal to Li_2S_6 (SOC = 25%), Li_2S_4 (SOC = 50%), and Li_2S_3 (SOC = 75%), respectively (red line in Fig. 2*C*). Interestingly, the XPS spectra showed that Li_2S, represented by S^{2-} at 160.7 eV, was generated immediately upon lithiation. In the nonaqueous Li–S battery, however, this fully lithiated form would only appear in the very late or even the last stage of lithiation, due to the slow reaction kinetics (6, 20). The early appearance of Li_2S in WiBS electrolyte confirms the rather fast kinetics for the lithiation reactions, and is consistent with a relatively flat charge–discharge profile. At the end of the lithiation (SOC = 100%), Li_2S expectedly becomes the dominant species (72%), in excellent agreement with the 79% of the theoretical capacity obtained previously. Meanwhile, XPS spectra also confirmed the formation of a LiF-rich SEI on anode surface, with a conspicuous change in F 1*s* peaks before and after 20 lithiation cycles. Similar conclusions can be drawn from high-resolution TEM images (*SI Appendix*, Figs. S5 and S6).

In summary, the S-KB composite in WiBS electrolyte seemed to follow a similar lithiation pathway to that in nonaqueous electrolyte, represented by the formation of predominant Li_2S_6, Li_2S_4, Li_2S_2, and Li_2S XPS peaks (8, 30), but with unprecedented fast kinetics. Short-chain LiPS species (Li_2S_x, $x < 6$) have been considered soluble in aqueous media (15), as confirmed by the formation of water-solvated species detected in the Raman spectra for lithium polysulfide. MD simulations also predict that

both solid Li_2S_2 and Li_2S_4 can take very small amount of water from WiBS electrolyte to form solid–liquid mixed semianolyte due to limited free-water in WiBS and large amount of Li_2S_2/Li_2S_4 (*SI Appendix*, Fig. S21). However, using both in situ Raman and mass spectra, we found that only a trace amount of liquid lithium polysulfide (<71 ppm) was observed to diffuse into the bulk electrolyte (*SI Appendix*, Figs. S7 and S8). SEM images and corresponding energy-dispersive X-ray spectroscopy of sulfur demonstrated little change in surface morphology of the S-KB anode (*SI Appendix*, Fig. S9). All these findings, along with the excellent electrochemical behavior, converged to one conclusion that the extremely high concentration of LiTFSI and LiOTf effectively expelled the liquefied short-chain lithium polysulfides from WiBS electrolyte.

In a visual manner, a simple dissolution experiment (Fig. 2*D*) was also carried out to demonstrate the negligible solubility of Li_2S powder and short-chain lithium polysulfide anolyte in WiBS electrolyte. The 4-M aqueous solutions of Li_2S_2 and Li_2S_4 with jacinth color (Fig. 2*D* and *SI Appendix*, Fig. S10*A*) were nominally formed with a 1:1 and 3:1 molar radio of sulfur to Li_2S aqueous solution by the following reaction:

$$Li_2S + S_{x-1} \leftrightarrow Li_2S_x (x < 6) \quad [1]$$

These lithium polysulfide solutions were mixed with a 28-mol·kg^{-1} WiBS electrolyte and allowed to stand for 2 or 24 h, respectively. As shown in Fig. 2*D*, a yellow boundary still existed between the two distinct phases, with the upper part being lithium polysulfide solutions due to their lower densities, and lower part being WiBS bulk electrolyte, as supported by their respective Raman spectra (*SI Appendix*, Fig. S11 *A* and *B*). To prove that such phase separation is thermodynamic, a more rigorous miscibility test was done for longer duration (5 d) at higher temperature (70 °C; *SI Appendix*, Fig. S10*B*) with the same results. Carefully examining the yellow interlayer between the aqueous solution of short-chain lithium polysulfide and WiBS electrolyte in Fig. 2*D*, we detected a cluster of white small solid particles, which had diffused from the yellow phase into the clear electrolyte phase after 24 h. A similar phenomenon was also observed in the full cell after long-term cycling (*SI Appendix*, Fig. S12*A*). These particles were collected by centrifugation and determined with Raman spectroscopy to be elemental sulfur (*SI Appendix*, Fig. S11*C*), which might have been generated from a disproportionation reaction of metastable polysulfides following the reverse direction of Eq. **1**. On both sides of the interface, Li_2S_x and LiTFSI/LiOTf should be nearly saturated, but inevitably cross-over of trace water still occurs at the interface, causing such disproportionation reaction.

Polysulfides dissolved in aqueous solutions have a tendency to hydrolyze rapidly and release hydrosulphide anion HS^- and/or H_2S, which would be hazardous from both battery performance and safety/environment considerations (17). This side reaction was found to be effectively suppressed in WiBS electrolyte system, because of the low activity of water molecules that are tightly bound by the high population of cations and anions. Quantum chemistry calculations also showed that such H-transfer reaction is energetically unfavorable for Li_2S_4 in WiBS, as shown in *SI Appendix*, Figs. S18–S20.

Electrochemical Performance of S-KB/$LiMn_2O_4$ Full Cells. A full cell of the previously unobserved Li^+/S chemistry was constructed using the S-KB anode coupled with a $LiMn_2O_4$ cathode (*SI Appendix*, Fig. S13*A*) in WiBS electrolyte, and its electrochemical behavior was evaluated at different current densities (Fig. 3*A*). The cathode/anode capacity ratio was set at 1.03:1, and the areal sulfur loadings in S-KB anode was set at a high value of ~8 mg·cm^{-2} (31). Remarkably, at a slow rate of 0.2C (discharge/charge of full theoretical capacity in 5 h), the cell being cycled between 2.2 and ~0.5 V exhibited a single discharge plateau with an average voltage of 1.60 V, delivering a discharge capacity of 84.40 mAh·g of total electrode mass (i.e., 1,327 mAh·g^{-1} of sulfur mass) or an areal capacity of 10.6 mAh·cm^{-2}. The energy density was conservatively estimated to be ~135 Wh/(kg of total electrode mass), which represents a marked improvement not only over all conventional aqueous Li-ion systems (<75 Wh·kg^{-1}) (9, 11), but in particular also over what was achieved by the highly concentrated aqueous electrolytes (12, 13, 18). At a rate five times higher (1C), the capacity dropped only slightly, to 68.24 mAh·g^{-1}, reflecting the fast kinetics of the cell reactions.

To examine the reaction kinetics of S-KB anodes, we performed galvanostatic intermittent titration experiments (GITT) (Fig. 3*B*) on an S-KB/$LiMn_2O_4$ full cell with the capacity of the $LiMn_2O_4$ cathode being in excess by five times to that of the S-KB anode. A constant current (0.1C) was applied as short pulses, between which the system was allowed to relax to quasi-equilibrium (*Materials and Methods*). Remarkably, a reversible capacity close to the theoretical value of sulfur (1,667 mAh·g^{-1}) was achieved during the first cycle under this quasi-equilibrium condition, which cannot be achieved in nonaqueous systems (32, 33). Moreover, the gap between the potential at the end of each pulse (polarization potential, as indicated by the black line in Fig. 3*B*) and the potential at the end of each relaxation (quasi-equilibrium potential, as indicated by the red line) were consistently low at 30–80 mV during most of the charge/discharge processes, except at the end of charge/discharge due to the increase in concentration polarization. This remarkably small overpotential further confirms the fast lithiation/delithiation kinetics of the S-KB anode in WiBS electrolyte. In sharp contrast, the lithiation process in typical nonaqueous electrolytes based on 1,3-dioxalane and dimethoxyethane normally undergoes three distinct stages with varying kinetics, which correspond to phase

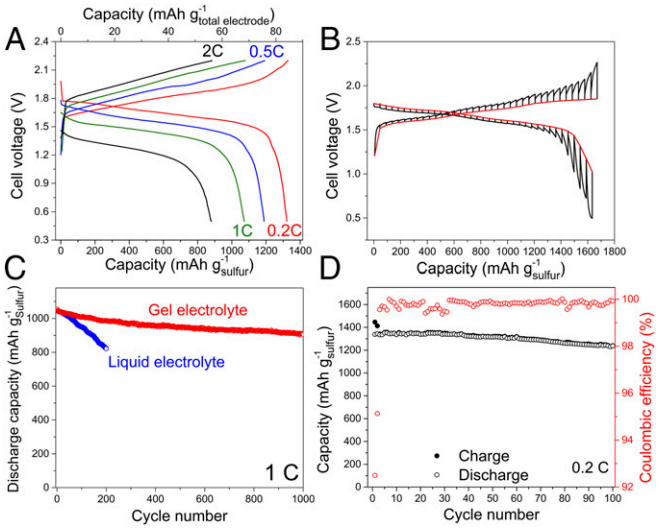

Fig. 3. Electrochemical performance of S-KB/$LiMn_2O_4$ full cells and S-KB cathodes. (*A*) Voltage profiles of full cell with S-KB anode and $LiMn_2O_4$ cathode in WiBS electrolyte at current densities ranging from 0.2 to 2C. The specific capacities were evaluated both by sulfur mass and total electrode (S and $LiMn_2O_4$) mass. (*B*) GITT characterization of S-KB cathode in WiBS electrolyte with five times higher capacity of $LiMn_2O_4$ cathode to avoid the interference by two plateaus of $LiMn_2O_4$. Red curve is quasi-equilibrium potential of sulfur at different lithiation/delithiation stages, which was constructed from the last data point of each open-circuit voltage period. (*C*) Corresponding cycling performance of aqueous S-KB/$LiMn_2O_4$ full cells with liquid and gel electrolytes at 1C rate; and (*D*) cycling stability of S-KB/$LiMn_2O_4$ full cells in aqueous gel electrolyte at low rate of 0.2C. The specific capacities were evaluated by sulfur mass.

changes from solid S_8 to soluble S_x^{2-} species ($x > 4$) followed by isolated solid Li_2S_x ($x = 2$ and 1) (32), accompanied by much higher potential hysteresis. A single-potential plateau similar to this work has been observed in the Li/S cell with a solid-state electrolyte (34), but still with much higher overpotential. The aqueous sulfur chemistry described in this work provides an avenue to exploit this cheap and energy-dense cathode material.

Cycling Performance of S-KB/LMO Full Cells. The cycling stability has always been an issue plaguing nonaqueous Li/S batteries, whose capacity fades rapidly due to the dissolution of polysulfide intermediates and the parasitic shuttling reactions thereafter, which result in self-discharge within the cell as well as continuous loss of active materials (30). However, in the 28-mol·kg^{-1} WiBS electrolyte, they are effectively suppressed because of the very limited free-water in WiBS and the phase separation between polysulfides and WiBS. The full Li-ion/sulfur cell in 28-mol·kg^{-1} WiBS electrolyte showed good cycling stability (Fig. 3*C*) due to the immobilization of the polysulfide species. However, a capacity decay of 22% still occurs over 200 cycles at 1C rate, indicating that the disproportionation reaction of lithium polysulfides still prevailed over the time due to cross-over of trace water at the interface. This side reaction slowly created elemental sulfur particles during repeated charge/discharge, leading to a major loss of active material (*SI Appendix*, Figs. S11*C* and S12*A*).

Further efforts were made to mitigate the generation and cross-over of elemental sulfur particles by immobilizing them in a "solidified" WiBS electrolyte with the formation of a polymeric gel. A hydrophilic polymer polyvinyl alcohol (PVA), which has been widely used as a matrix in solid-state supercapacitors (35, 36), was introduced into the WiBS electrolyte to form a hydrogel (*SI Appendix*, Fig. S14 *A* and *B*). Unexpected high solubility of PVA (mass ratio of PVA to water > 0.8:1) suggested that PVA chain with abundant hydroxyl groups, which also possess solvation power, must have interacted with lithium salts. The FTIR (*SI Appendix*, Fig. S14*C*) of this gel polymer electrolyte (GPE) is almost identical to its parental aqueous electrolyte, and there is also little difference in ion conduction as well as interphasial behavior between the GPE and its parental aqueous electrolyte (*SI Appendix*, Fig. S14*D*), as evidenced by almost identical electrochemical impedance spectroscopy in the course of 50 cycles (*SI Appendix*, Fig. S15). The S-KB/$LiMn_2O_4$ in this 28-mol·kg^{-1} WiBS-GPE exhibited almost identical charge/discharge profiles as that of 28-mol·kg^{-1} WiBS liquid electrolyte (*SI Appendix*, Fig. S14*F*). The hydrophilic polymer matrix, however, is expected to further interact with the lithium salts dissolved in WiBS, and repels the polysulfide anions, providing a chemical barrier to the sulfur loss into the bulk aqueous electrolyte (*SI Appendix*, Fig. S12*B*). With PVA polymer bonding with both water molecule and Li salts, the cross-over of trace water was significantly minimized, and the disproportionation reaction of LiPS essentially eliminated. This approach effectively maintains the sulfur in an active electrochemical state, thus significantly reducing capacity decay to 7% in the first 200 cycles at 1C. More importantly, after 1,000 cycles at 1C, the capacity still retained 86% of its initial value, corresponding to a very small capacity decay of 0.014% per cycle (Fig. 3*C*). This low fading rate is the best observed among all lithium/sulfur batteries, either nonaqueous or aqueous (5, 7). Even at a low charge/discharge rate of 0.2C, which has always been a challenge not only for the Li/S system but for all aqueous systems, the capacity decay was still only 9% after 100 cycles (Fig. 3*D*). During the SEI formation on the anode surface in the initial several cycles, Coulombic efficiency quickly increased from 92.49% in the first cycle, to 95.4% in the second cycle, then to 99.95 at the 30th cycle, and eventually reached ~100% after 40 cycles. Such high Coulombic efficiency ensures the long cycle stability. The effectiveness of this strategy in suppressing the side reaction was also evaluated by measuring the self-discharge rate of a Li^+/S cell at 100% SOC (*SI Appendix*, Fig. S16). As expected, a pronounced increase in retained discharge capacity was observed after a 24-h open-circuit voltage relaxation.

High Energy Density S-KB/HV-$LiCoO_2$ Full Cells. We have already constructed a unique Li^+/S battery based on this unique sulfur chemistry, which, with sulfur coupled with a $LiMn_2O_4$ cathode in WiBS electrolyte, achieved a gravimetric energy density of 135 Wh/(kg of total electrode mass) and a volumetric energy densities of ~384 Wh/(L of total electrode and electrolyte). It should be noted that the energy density of the S-KB/$LiMn_2O_4$ cell is limited by the $LiMn_2O_4$ due to its low potential and moderate capacity. For practical applications where high energy density is desired, cathode candidates with higher specific capacity and redox potential should be further explored (Fig. 4*A*). For instance, high-voltage $LiCoO_2$ (HV-$LiCoO_2$) with a capacity of 170 mAh·g^{-1} (*SI Appendix*, Fig. S13*B*) would make a better cathode in this aqueous sulfur battery (37), raising the energy density to an unprecedentedly high level for aqueous batteries. Indeed, such a full cell based on HV-$LiCoO_2$ cathode and S-KB anode delivered a stable discharge capacity of 119 mAh/(g of total electrode mass) with an average voltage of 1.64 V at 0.2C, leading to a gravimetric energy density of 195 Wh/(kg of total electrode mass) and a volumetric energy densities of ~454 Wh/(L of total electrode and electrolyte volume; Fig. 4*B*). With further optimization and engineering in cell design, the theoretical

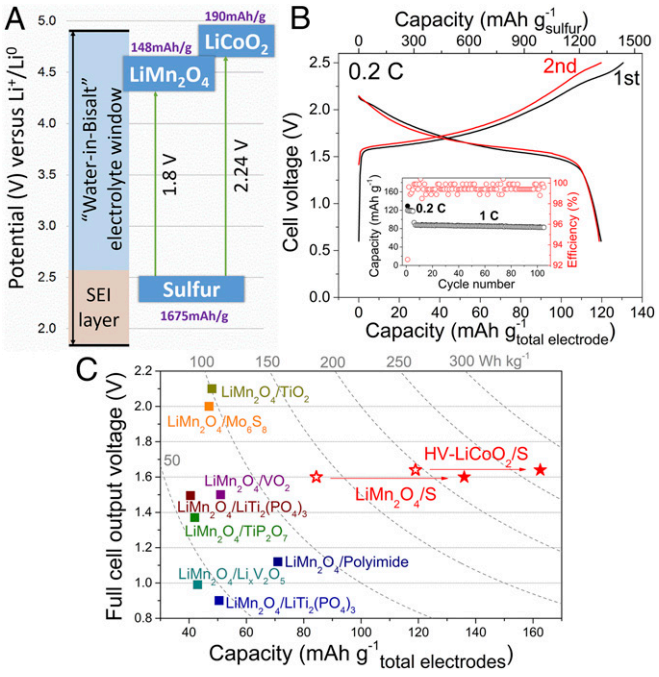

Fig. 4. Energy densities of aqueous Li-ion batteries. (*A*) Illustration of S/$LiMn_2O_4$ and S/HV-$LiCoO_2$ full cell in WiBS electrolyte with expanded electrochemical stability window. (*B*) Voltage profiles of S/HV-$LiCoO_2$ full cell in WiBS GPE at rate of 0.2C. (*Inset*) Capacity stability and coulombic efficiency during cycling. The specific capacities were evaluated by both sulfur mass and total electrode mass. (*C*) Comparisons of theoretical (closed stars) and actual (open stars) voltages, capacities, and energy densities of aqueous Li^+/S batteries with all reported aqueous electrochemical couples (squares). All of the gravimetric capacities and energy densities are based on the total weight of positive and negative electrodes, including the active materials, carbon additives, and binders (electrolyte and cell packaging were not considered). The theoretical material capacities and voltages were used for calculating the theoretical energy densities. The actual energy densities of the $LiMn_2O_4$/S and HV-$LiCoO_2$/S cells were experimentally obtained.

value of 267 Wh·kg^{-1} for the sulfur/HV-$LiCoO_2$ couple (Fig. 4*C*) could be eventually achieved. This highest value of energy density ever achieved in aqueous batteries is already approaching the commercial LIB chemistry (*SI Appendix*, Table S2), along with much superior safety.

As an overview of the state-of-the-art, in Fig. 4*C* we compared our aqueous Li^+/S batteries against other successful aqueous systems reported previously. In most cases, energy densities for aqueous systems were below 78 Wh·kg^{-1} (10, 38–40). The high-voltage aqueous Li-ion systems achieved in WiS electrolyte can deliver higher-energy density between 84 and 101 Wh·kg^{-1} (12, 13), although Yamada et al. (18) raised this value to ∼130 Wh·kg^{-1} by coupling lithiated titanate with $LiCoO_2$. Even higher energy density (183 Wh·kg^{-1} based on the weight of active electrode materials) became possible when Zn^{2+} and Li^+ chemistries are hybridized (41). It should be noted that the value of ∼200 Wh·kg^{-1} obtained from S/$LiCoO_2$ couple is already higher than some nonaqueous Li-ion batteries, e.g., $LiMn_2O_4$/$Li_4Ti_5O_{12}$ (160 Wh·kg^{-1}).

Conclusion

We demonstrated a unique sulfur chemistry in superconcentrated aqueous electrolyte, which delivers a close-to-theoretical capacity and fast reaction kinetics. We believe that, with the judicious choice of proper cathodes with higher capacities or potentials, the energy densities of the intrinsically safe and green aqueous rechargeable batteries could be further increased, eventually challenging the commercial nonaqueous LIBs (theoretical energy density of 150∼400 Wh·kg^{-1}), especially in applications where the needs for safety, low cost, and low toxicity outweigh those for high energy and power densities. Further efforts should be focused on cost reduction of WiBS electrolyte, making the Li-ion/sulfur battery closer to practical applications. The promising approaches might include alternative low-cost salts with the potentials to form similar phase separation, together with optimized cell engineering.

Materials and Methods

S-KB composite was obtained by thermal treatment to incorporate sulfur into the porous matrix. The electrodes were fabricated by compressing the mixture of active material powder, carbon black, and polytetrafluoroethylene (PTFE) on metal grid current collectors. WiBS aqueous electrolytes were prepared by dissolving 21 mol·kg^{-1} LiTFSI and 7 mol·kg^{-1} LiOTf salts in water. Aqueous gel electrolytes were prepared by further dissolving 10 wt % polyvinyl alcohol in the liquid WiBS electrolyte at 95 °C. More details of the materials used and methods followed are provided in *SI Appendix*.

ACKNOWLEDGMENTS. Funding for this work was provided by Department of Energy Advanced Research Projects Agency - Energy Grant DEAR0000389 (to C.W. and K.X.) and National Aeronautics and Space Administration (NASA) through the interagency agreement NND16AA29I (to O.B.).

1. Tarascon JM, Armand M (2001) Issues and challenges facing rechargeable lithium batteries. *Nature* 414:359–367.
2. Larcher D, Tarascon JM (2015) Towards greener and more sustainable batteries for electrical energy storage. *Nat Chem* 7:19–29.
3. Whittingham MS (2004) Lithium batteries and cathode materials. *Chem Rev* 104: 4271–4301.
4. Ji X, Lee KT, Nazar LF (2009) A highly ordered nanostructured carbon-sulphur cathode for lithium-sulphur batteries. *Nat Mater* 8:500–506.
5. Seh ZW, et al. (2014) Two-dimensional layered transition metal disulphides for effective encapsulation of high-capacity lithium sulphide cathodes. *Nat Commun* 5:5017.
6. Su YS, Fu Y, Cochell T, Manthiram A (2013) A strategic approach to recharging lithium-sulphur batteries for long cycle life. *Nat Commun* 4:2985.
7. Seh ZW, et al. (2013) Sulphur-TiO2 yolk-shell nanoarchitecture with internal void space for long-cycle lithium-sulphur batteries. *Nat Commun* 4:1331.
8. Zhang S, Ueno K, Dokko K, Watanabe M (2015) Recent advances in electrolytes for lithium-sulfur batteries. *Adv Energy Mater* 5:1500117.
9. Kim H, et al. (2014) Aqueous rechargeable Li and Na ion batteries. *Chem Rev* 114: 11788–11827.
10. Li W, Dahn JR, Wainwright DS (1994) Rechargeable lithium batteries with aqueous electrolytes. *Science* 264:1115–1118.
11. Wang Y, Yi J, Xia Y (2012) Recent progress in aqueous lithium-ion batteries. *Adv Energy Mater* 2:830–840.
12. Suo L, et al. (2015) "Water-in-salt" electrolyte enables high-voltage aqueous lithium-ion chemistries. *Science* 350:938–943.
13. Suo L, et al. (2016) Advanced high-voltage aqueous lithium-ion battery enabled by "Water-in-Bisalt" electrolyte. *Angew Chem Int Ed Engl* 55:7136–7141.
14. Licht S (1988) Aqueous solubilities, solubility products and standard oxidation-reduction potentials of the metal sulphides. *J Electrochem Soc* 135:2971–2975.
15. Li N, et al. (2014) An aqueous dissolved polysulfide cathode for lithium-sulfur batteries. *Energy Environ Sci* 7:3307–3312.
16. Demir-Cakan R, Morcrette M, Leriche JB, Tarascon JM (2014) An aqueous electrolyte rechargeable Li-ion/polysulfide battery. *J Mater Chem A Mater Energy Sustain* 2:9025–9029.
17. Visco SJ, et al. (2014) US Patent US8828575 B2.
18. Yamada Y, et al. (2016) Hydrate-melt electrolytes for high-energy-density aqueous batteries. *Nat Energy* 1:16129.
19. Jayaprakash N, Shen J, Moganty SS, Corona A, Archer LA (2011) Porous hollow carbon@sulfur composites for high-power lithium-sulfur batteries. *Angew Chem Int Ed Engl* 50:5904–5908.
20. Pang Q, Kundu D, Cuisinier M, Nazar LF (2014) Surface-enhanced redox chemistry of polysulphides on a metallic and polar host for lithium-sulphur batteries. *Nat Commun* 5:4759.
21. Yamin H, Gorenshtein A, Penciner J, Sternberg Y, Peled E (1988) Lithium sulfur battery: oxidation/reduction mechanisms of polysulfides in THF solutions. *J Electrochem Soc* 135:1045–1048.
22. Ji X, Nazar LF (2010) Advances in Li-S batteries. *J Mater Chem* 20:9821–9826.
23. Mikhaylik YV, Akridge JR (2004) Polysulfide shuttle study in the Li/S battery system. *J Electrochem Soc* 151:A1969–A1976.
24. Yeon JT, et al. (2012) Raman spectroscopic and X-ray diffraction studies of sulfur composite electrodes during discharge and charge. *J Electrochem Soc* 159: A1308–A1314.
25. Janz GJ, Coutts JW, Downey JR, Roduner E (1976) Raman studies of sulfur-containing anions in inorganic polysulfides. Potassium polysulfides. *Inorg Chem* 15:1755–1759.
26. Smith LC, et al. (2016) Sol–gel encapsulated lithium polysulfide catholyte and its application in lithium–sulfur batteries. *Mater Horiz* 3:137–144.
27. Wu HL, Huff LA, Gewirth AA (2015) In situ Raman spectroscopy of sulfur speciation in lithium-sulfur batteries. *ACS Appl Mater Interfaces* 7:1709–1719.
28. Fantauzzi M, Elsener B, Atzei D, Rigoldi A, Rossi A (2015) Exploiting XPS for the identification of sulphides and polysulfides. *RSC Advances* 5:75953–75963.
29. Helen M, et al. (2015) Single step transformation of sulphur to Li2S2/Li2S in Li-S batteries. *Sci Rep* 5:12146.
30. Bruce PG, Freunberger SA, Hardwick LJ, Tarascon JM (2011) Li-O_2 and Li-S batteries with high energy storage. *Nat Mater* 11:19–29.
31. Qie L, Zu C, Manthiram A (2016) A high energy lithium-sulfur battery with ultrahigh-loading lithium polysulfide cathode and its failure mechanism. *Adv Energy Mater* 6:1502459.
32. Busche MR, et al. (2014) Systematical electrochemical study on the parasitic shuttle-effect in lithium-sulfur-cells at different temperatures and different rates. *J Power Sources* 259:289–299.
33. Park J-W, et al. (2013) Solvent effect of room temperature ionic liquids on electrochemical reactions in lithium-sulfur batteries. *J Phys Chem C* 117:4431–4440.
34. Cuisinier M, et al. (2014) Unique behaviour of nonsolvents for polysulfides in lithium–sulfur batteries. *Energy Environ Sci* 7:2697–2705.
35. Peng X, et al. (2016) A zwitterionic gel electrolyte for efficient solid-state supercapacitors. *Nat Commun* 7:11782.
36. Wu C, et al. (2013) Two-dimensional vanadyl phosphate ultrathin nanosheets for high energy density and flexible pseudocapacitors. *Nat Commun* 4:2431.
37. Chen Z, Dahn JR (2004) Methods to obtain excellent capacity retention in $LiCoO_2$ cycled to 4.5 V. *Electrochim Acta* 49:1079–1090.
38. Wang H, Huang K, Zeng Y, Yang S, Chen L (2007) Electrochemical properties of TiP_2O_7 and $LiTi_2(PO_4)_3$ as anode material for lithium ion battery with aqueous solution electrolyte. *Electrochim Acta* 52:3280–3285.
39. Wang H, Zeng Y, Huang K, Liu S, Chen L (2007) Improvement of cycle performance of lithium ion cell $LiMn_2O_4$/$Li_xV_2O_5$ with aqueous solution electrolyte by polypyrrole coating on anode. *Electrochim Acta* 52:5102–5107.
40. Luo JY, Cui WJ, He P, Xia YY (2010) Raising the cycling stability of aqueous lithium-ion batteries by eliminating oxygen in the electrolyte. *Nat Chem* 2:760–765.
41. Zhao J, et al. (2016) High-voltage Zn/$LiMn_{0.8}Fe_{0.2}PO_4$ aqueous rechargeable battery by virtue of "water-in-salt" electrolyte. *Electrochem Commun* 69:6–10.